RSC Advances

PAPER

View Article Online
View Journal | View Issue

Cite this: RSC Adv., 2017, 7, 41540

Gas–solid reaction for *in situ* deposition of Cu_3SbS_4 on a mesoporous TiO_2 film†

Yu Zhang,[ab] Jianhua Tian,[a] Kejian Jiang,*[b] Jinhua Huang,[b] Huijia Wang[ab]
and Yanlin Song*[b]

Received 24th July 2017
Accepted 20th August 2017

DOI: 10.1039/c7ra08137e

rsc.li/rsc-advances

Herein, a novel, facile, *in situ* gas–solid reaction method has been successfully employed for the deposition of famatinite (Cu_3SbS_4) semiconductor on a mesosporous TiO_2 film, where precursors $CuCl_2$ and $SbCl_3$ were first solution-coated on a TiO_2 substrate, followed by reaction with H_2S gas and further thermal annealing. Various precursor ratios, temperatures and heating atmospheres have been examined for the deposition. The phase-pure Cu_3SbS_4 has been obtained by coating a mixed solution of $CuCl_2$ and $SbCl_3$ at a molar ratio of 2.5 : 1, and annealing at 300 °C for 10 min in an H_2S atmosphere. The deposited Cu_3SbS_4 was uniformly distributed on the entire porous TiO_2 film with crystal grain sizes of about 3–4 nm. X-ray photoelectron spectroscopy (XPS) analysis revealed valence states of the synthetic samples for Cu^+, Sb^{5+} and S^{2-}, verifying phase-pure Cu_3SbS_4. The spectral absorption of the film ranges from 400 nm to 1000 nm with a band gap of ~1.24 eV. The Cu_3SbS_4 film shows good and stable photoresponse performance, indicating its high potential as photovoltaic absorber.

Introduction

Thin film solar cells based on CdTe[1] and $Cu(In_{1-x}Ga_x)Se$ (CIGS)[2] have drawn much attention due to their excellent absorbance and high efficiencies of nearly 20%. Despite their success, these materials contain toxic (cadmium) and less-abundant elements (tellurium, indium, and gallium). Therefore, cheap, low-toxicity, and earth-abundant metal sulfide semiconductors, such as $Cu_2ZnSn(S, Se)_4$ (CZTSSe),[3–5] Fe_2S,[6,7] Cu_2FeSnS_4 (ref. 8–10) and SnS[11,12] have increasingly attracted attention as promising alternatives.

Cu–Sb–S ternary compounds, including four major phases: $CuSbS_2$ (chalcostibite),[13–16] $Cu_{12}Sb_4S_{13}$ (tetrahedrite),[17,18] Cu_3SbS_4 (famatinite),[19–21] and Cu_3SbS_3 (skinnerite),[22,23] have also emerged as potential absorber materials because of their appropriate optical, electrical properties and the presence of earth-abundant elements.[22] Among them, Cu_3SbS_4 is suggested as a promising light absorber with an optimum band gap energy of ~1.1 eV, comparable with those of high-efficiency CIGS and CZTSSe materials.[24] In the past years, various solution techniques have been explored for the preparation of nano/microscale Cu_3SbS_4 particles.[18,22,24,25] In 2013, J. Embden[18] reported the synthesis of $Cu_{12}Sb_4S_{13}$ and Cu_3SbS_4 nanocrystals through optimizing the ligand chemistry in a hot-injection reaction. Moreover, colloidal nanocrystals of the four different Cu–Sb–S phases were obtained through adjusting the ratios of the precursors and reaction temperatures in the hot-injection method.[22] Besides, G. Chen[26] studied the synthesis and formation mechanism of flower-like Cu_3SbS_4 particles *via* microwave irradiation. In contrast, there were few reports on the *in situ* preparation of Cu_3SbS_4 polycrystalline films. Franzer[27] reported fabrication of polycrystalline Cu_3SbS_4 films by magnetron sputtering. Very recently, U. Chalapathi[20] reported on the fabrication of Cu_3SbS_4 thin film by annealing the Sb_2S_3/CuS stacking layers, where both the Sb_2S_3 and CuS thin films with appropriate thicknesses are deposited by a chemical bath deposition technique. Both the methods, however, remain inherent disadvantages such as requisite high vacuum or difficulty in the control of the film with desired stoichiometric composition.

Recently, we developed a simple, low-cost, *in situ* gas–solid reaction method for the deposition of binary metal sulfide Sb_2S_3, CdS, and ternary $CuSbS_2$.[28–30] In this approach, a precursor salt was first introduced from solution into a nanoporous TiO_2 film, and subsequently transformed into sulfide through reaction with H_2S.[28–30] Herein, we further extended this method for the fabrication of Cu_3SbS_4 film. Through optimizing different precursor concentrations, temperatures and heating atmosphere, pure-phase Cu_3SbS_4 was achieved. The optical and electrical properties proved that the Cu_3SbS_4 film could be used as an attractive light absorber in photovoltaics.

---

[a] School of Chemical Engineering and Technology, Tianjin University, Tianjin 300072, P. R. China

[b] Key Laboratory of Green Printing, Institute of Chemistry, Chinese Academy of Sciences, Beijing 100190, P. R. China. E-mail: kjjiang@iccas.ac.cn; ylsong@iccas.ac.cn

† Electronic supplementary information (ESI) available. See DOI: 10.1039/c7ra08137e

Experimental

Fabrication of TiO_2/Cu_3SbS_4 device

First, the soda-lime glasses were cleaned by ultrasonic treatment with detergent, deionized water, ethanol and acetone successively, and then blow-dried by nitrogen gas. 20 nm-sized TiO_2 paste (DSL 18NM-T, Dyesol), diluted with ethanol as a mass ratio of 1 : 1.5, was blade coated on the cleaned glass substrates, followed by calcination at 125 °C for 5 min and 500 °C for 30 min. For the deposition of Cu_3SbS_4, various ethanolic solutions of $CuCl_2$ and $SbCl_3$ were prepared with the molar ratios of Cu : Sb set as 2 : 1, 2.3 : 1, 2.5 : 1, and 3 : 1. The precursor solution was first dropped on the mesoporous TiO_2 film and kept for 10 s, then spin-coated at 2000 rpm for 20 s. After the coating, the film was rapidly put in an enclosed quartz container full of H_2S gas (Fig. 1), which was generated by reaction of 20 wt% sodium sulfide ($Na_2S\cdot 9H_2O$) and 10 wt% dilute sulfuric acid (H_2SO_4). With the addition of Na_2S solution in the dilute H_2SO_4, H_2S gas was generated and entered into the reaction vessel. The TiO_2 film turned dark brown in color upon the addition. After 2 minutes, the film was taken out, washed by ethanol to remove the remnant and resulting by-products, then blown by nitrogen. Afterwards, the film was moved into the quartz container again, and annealed on a hot plate at different temperatures from 200 to 350 °C for 10 min.

Fabrication of Cu_3SbS_4 device

Fluorine-doped SnO_2 (FTO) substrates with a resistivity of $\sim 10\ \Omega\ cm^{-1}$ were cleaned with detergent, deionized water, ethanol and acetone successively. On the substrate, a dense titanium dioxide film was prepared as barrier layer to prevent short circuiting through sequentially deposition and annealing of 0.15 M and 0.3 M titanium (diisopropoxide) bis(2,4-pentanedionate) solutions in *n*-butanol. The TiO_2/Cu_3SbS_4 films were prepared with above-mentioned procedure. Finally, a 60 nm-thick silver (Ag) was deposited on the film as counter electrode by thermal evaporation.

Characterization

Cu_3SbS_4 thin films were characterized by X-ray diffraction (XRD) using a Bruker D8 Discover diffractometer (with Cu Kα radiation at 1.540598 Å). The surface morphologies and X-ray energy-dispersive spectrometer (EDS) of the Cu_3SbS_4 thin films were investigated by a field-emission scanning electron microscope (JSM-7500, Japan) and the transmission electron microscopy (TEM) images were acquired with a JEOL HT7700 microscope. X-ray photoelectron spectroscopy (XPS) were performed on the Thermo Scientific ESCA Lab 250Xi using 200 W monochromated Al Kα radiation, and 500 μm X-ray spot was used for XPS analysis. Typically the hydrocarbon C 1s line at 284.8 eV from adventitious carbon is used for energy referencing. The absorption spectra were measured using a UV/Vis/NIR spectrometer (PerkinElmer Lambda 950) and Raman spectrum were recorded on a Bruker Fourier Raman spectrometer (RFS100/S) with a laser excitation wavelength of 532 nm. Ultraviolet photoelectron spectroscopy (UPS) measurement was made on a Specs UVLS using He I excitation (21.15 eV, referenced to the Fermi edge of argon etched gold). The photoresponse performance was conducted on a computer-controlled Keithley 2400 under the illumination of AM 1.5 G. The applied voltage was 20 mV and active area of the device was 0.04 cm^{-2}.

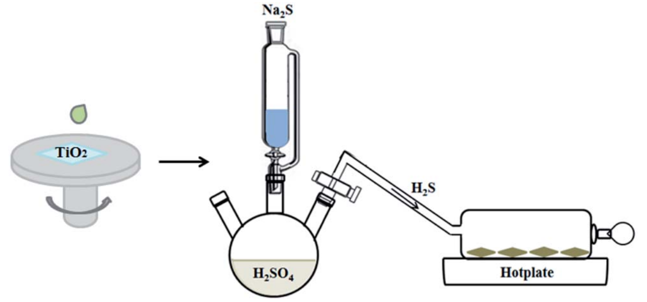

Fig. 1 Schematic diagram of fabrication procedure for Cu_3SbS_4 film.

Results and discussion

Preparation for pure-phase Cu_3SbS_4 film

Fig. 2 shows XRD patterns (a) and Raman spectra (b) of Cu_3SbS_4 film prepared with molar ratios of Cu : Sb set at 2 : 1, 2.3 : 1, 2.5 : 1, and 3 : 1, respectively. As shown in Fig. 2(a), the XRD pattern for the 2.5 : 1 film presents the diffraction peaks at $2\theta =$ 28.70°, 47.78°, 56.66° and 64.75°, corresponding to (112), (204), (312) and (314) faces of famatinite Cu_3SbS_4 pattern (JCPDS 35-0581).[22] All the peaks neither match with those of Sb_2S_3 or CuS,[31,32] nor the peaks of other crystalline structures, such as $CuSbS_2$ (chalcostibite), $Cu_{12}Sb_4S_{13}$ (tetrahedrite) and Cu_3SbS_3 (skinnerite),[24] indicating the complete conversion of $CuCl_2$ and $SbCl_3$ with the ratio at 2.5 : 1. At lower ratios of 2 : 1 and 2.3 : 1, several weak peaks from Sb_2S_3 can be distinguished, while at the higher ratio of 3 : 1, the peaks for Sb_2S_3 disappeared, but new peaks for CuS appeared together with those from Cu_3SbS_4. Thus, phase-pure Cu_3SbS_4 could be obtained only at the ratio of around 2.5 : 1. The deviation from the stoichiometric composition of Cu_3SbS_4 (3 : 1) could be explained as follows. In the initial stage of the reaction between the Cu^{2+}/Sb^{3+} and H_2S, CuS and Sb_2S_3 formed at room temperature, as shown in eqn (1) and (2). During the annealing, the CuS and Sb_2S_3 reacted to form Cu_3SbS_4, as shown in eqn (3). In this process, Sb_2S_3 could gradually volatilize due to its effumability. Therefore, a little excess of Sb^{3+} precursor is essential to obtain pure Cu_3SbS_4 phase.

$$CuCl_2 + H_2S \rightarrow CuS + 2HCl\uparrow \tag{1}$$

$$2SbCl_3 + 3H_2S \rightarrow Sb_2S_3 + 6HCl\uparrow \tag{2}$$

$$6CuS + Sb_2S_3 \rightarrow 2Cu_3SbS_4 + S\uparrow \tag{3}$$

The Raman spectrum of the 2.5 : 1 film shows shifts at 147, 198, 246, 273, 319, 345, 398, 515 cm^{-1} and 637 cm^{-1}. Here, the peaks of 246, 273, 319, 345 cm^{-1} and 637 cm^{-1} are close to those

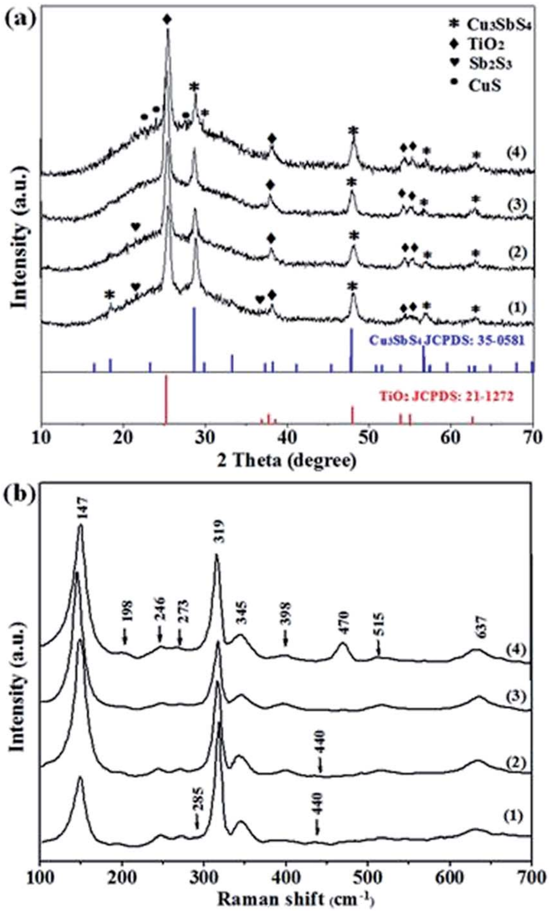

Fig. 2 XRD patterns (a) and Raman spectra (b) of Cu_3SbS_4 film prepared by different precursor ratio of 2 : 1 (1), 2.3 : 1 (2), 2.5 : 1 (3) and 3 : 1 (4) at 300 °C calcination.

of Cu_3SbS_4 phase,[20] while the peaks of 147, 198, 398 cm^{-1} and 515 cm^{-1} are from the TiO_2 substrate.[33] Notably, a distinct peak at 470 cm^{-1} can be noticed in the spectrum of the 3 : 1 film, due to the presence of the excess CuS.[31] In the case for the 2 : 1 and 2.3 : 1 films, a few of weak peaks are observed at 285 and 440 cm^{-1} from Sb_2S_3.[34] The results are consistent with the phase analysis of XRD. Besides, the elemental composition and EDS spectra of the Cu–Sb–S films are presented in Table 1 and Fig. S1.† It is clear that at the ratio of 2.5 : 1, the average Cu/Sb/S elemental ratio (2.73 : 0.92 : 3.70) is very close to the stoichiometric value of 3 : 1 : 4 of Cu_3SbS_4. All the results indicate that phase-pure Cu_3SbS_4 film can be synthesized with $CuCl_2$ and $SbCl_3$ at the ratio of 2.5 : 1 by *in situ* gas–solid reaction method.

Table 1 Elemental composition of Cu_3SbS_4 film prepared by different precursor ratio of 2 : 1, 2.3 : 1, 2.5 : 1 and 3 : 1 (from SEM-EDX)

Ratio	2 : 1	2.3 : 1	2.5 : 1	3 : 1
Cu (%)	2.97	4.12	2.73	3.27
Sb (%)	1.15	1.43	0.92	0.95
S (%)	4.10	5.27	3.70	3.90

In previous reports, reaction temperature was regarded as an pivotal factor for controlling the ternary phase composition and crystallinity.[5,20] Here, various annealing temperatures ranged from 200 °C to 350 °C were examined, and the corresponding XRD patterns were shown in Fig. 3. The peak intensity for Cu_3SbS_4 at $2\theta = 28.70°$, 33.33°, 47.78°, 56.66° and 64.75° are very weak when annealing at 200 °C for 10 min, implying poor crystallinity under this condition.[26] Increasing the temperature to 300 °C, the crystallinity is evidently improved with the enhanced intensity of all the peaks. With further increasing the temperature to 350 °C, new peaks for CuS appeared. The observation may imply that at this high temperature annealing, the Cu_3SbS_4 was partially decomposed to CuS and Sb_2S_3, and the resulting CuS remained after volatilization of the Sb_2S_3. Besides, different atmosphere could affect the crystal phases during the annealing (Fig. 4). Here, the annealing was carried out under H_2S or N_2 atmosphere, respectively. Different from in H_2S atmosphere, where only pure Cu_3SbS_4 phase appeared, both Cu_3SbS_4 and $CuSbS_2$ phases were observed under N_2 annealing ambience. The result implies that H_2S environment is requisite to supply adequate amount of S element and avoid the formation of other Cu–Sb–S phases due to the loss of S element during the annealing. All the results demonstrated that pure famatinite Cu_3SbS_4 film was achieved by the *in situ* gas–solid reaction with $Cu^{2+} : Sb^{3+}$ at the ratio of 2.5 : 1 and annealing in H_2S at 300 °C for 10 min. Here, the film prepared with the ratio at 2.5 : 1 is named as 2.5 : 1 film for further investigation.

XPS analysis was carried out to investigate the elemental state and composition of the 2.5 : 1 film. From the full analysis of XPS spectrum (Fig. 5(a)), no peaks were observed for any other elements except Cu, Sb, S, Ti, O and C. Here, carbon element is adventitious used for energy referencing, and the peaks for Ti and O are attributed to porous TiO_2 substrate. The spectrum of Cu (Fig. 5(b)) shows two Gaussian peaks at

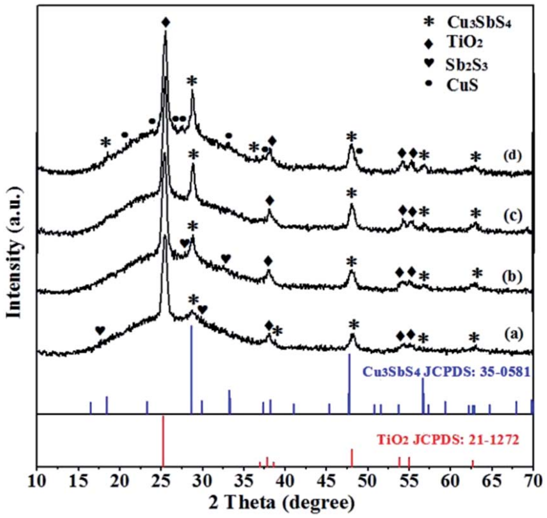

Fig. 3 XRD patterns of Cu_3SbS_4 film as a precursor ratio of 2.5 : 1 heated at different temperatures for 10 min: 200 °C (a), 250 °C (b), 300 °C (c), 350 °C (d).

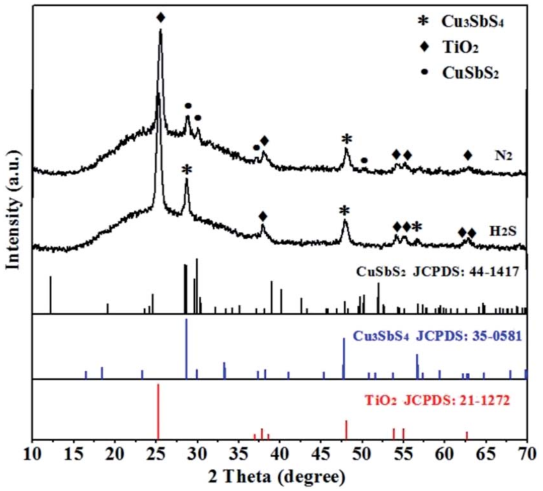

Fig. 4 XRD patterns of Cu_3SbS_4 film as a precursor ratio of 2.5 : 1 heated at H_2S and N_2 atmosphere at 300 °C for 10 min.

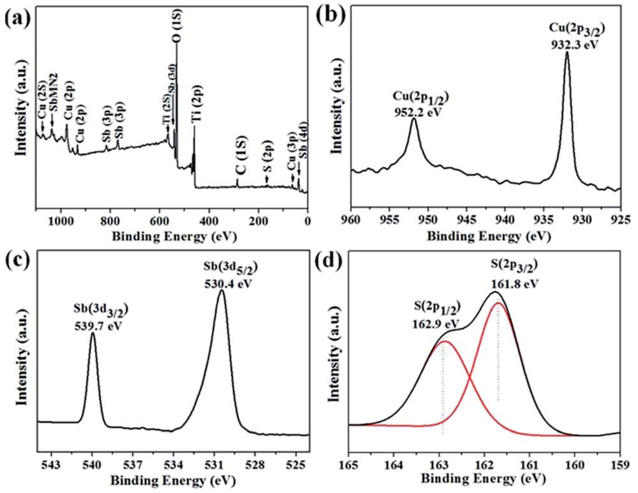

Fig. 5 X-ray photoelectron spectra (XPS) survey scan (a), Cu (2p) (b), Sb (3d) (c), and S (2p) (d) core levels of 2.5 : 1 film and heat treatment in H_2S at 300 °C.

952.2 and 932.3 eV with a separation of 19.9 eV, which are corresponding to Cu $2p_{1/2}$ and Cu $2p_{3/2}$ binding state, respectively. The above binding energies are well consistent with reported values for Cu^+.[35] The antimony presents doublet at the binding energies at 539.7 eV ($3d_{3/2}$) and 530.4 eV ($3d_{5/2}$), which are in good agreement with those of Sb^{5+}, and no peaks are observed at 538.7 and 529.2 eV for Sb^{3+}.[20,36] The peaks at 162.9 and 161.8 eV represent the S $2p_{1/2}$ and $2p_{3/2}$, respectively, which are consistent with the chemical state of sulfur (S^{2-}) in the Cu_3SbS_4. Thus, XPS analysis indicates that the elemental state of the 2.5 : 1 film are $(Cu^+)_3(Sb^{5+})(S^{2-})_4$.

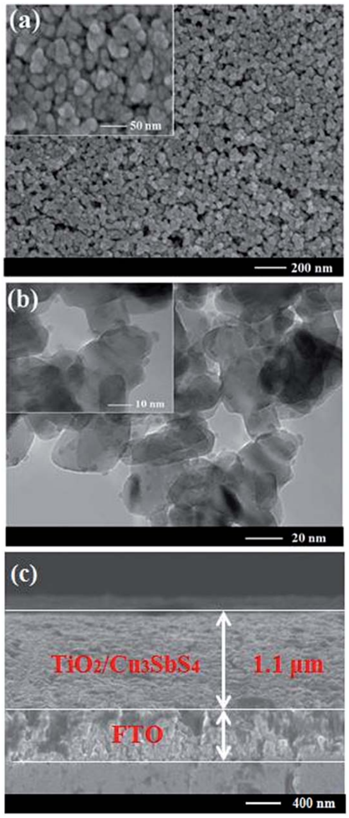

Fig. 6 Top-view SEM (a), TEM (b) and cross sectional SEM (c) images of Cu_3SbS_4 film prepared by *in situ* gas–solid reaction method as a precursor ratio of 2.5 : 1 film and heat treatment in H_2S at 300 °C.

The microstructure of the 2.5 : 1 film was further evaluated by recording the SEM and TEM images (in Fig. 6). According to the top-view SEM, uniform morphology is evident with many tiny Cu_3SbS_4 particles homogeneously distributed within the TiO_2 film, where the specific particle size could hardly be distinguished. In the TEM, lots of small granules of Cu_3SbS_4 can be observed on the surface of 20 nm TiO_2 balls with crystal grain sizes of about 3–4 nm. Besides, the cross sectional SEM (Fig. 6(c)) displays the thickness of TiO_2/Cu_3SbS_4 is about 1.1 μm. From the cross section, the mapping images were recorded, as shown in Fig. S2,† manifesting the homogeneous deposition of Cu, Sb and S elements in the TiO_2 film.

The determination of band gap and positions are significant for a potential photovoltaic absorber material. The UV-Vis-NIR absorption spectrum of Cu_3SbS_4 film shows a wide absorption range from 400 nm to 1000 nm. The $(\alpha h\nu)^{1/2}$ *versus* $h\nu$ curves (Tauc plots, inset of Fig. 7(a)) is plotted, and band gap is estimated to be 1.24 eV, which is closed to the reported band gap of 1.2 eV for Cu_3SbS_4.[22,26] Moreover, UPS was applied to determine valance band and Fermi energies of this film. From intercept of 16.54 eV for secondary electron onset and Au energy of 21.15 eV, Fermi energy position relative to vacuum is calculated to be −4.61 eV. The distance between Fermi energy and valance band is 0.25 eV by extrapolating and linear fitting the long tail of UPS spectrum. Combining with the band gap of 1.24 eV estimated from UV-Vis-NIR spectra, the valence band edge and conduction band edge are determined to be located at 4.86 eV and 3.62 eV relative to vacuum, respectively, which suggests its potential application as one kind of solar absorber materials.[17,37] The band alignment diagrams of TiO_2/Cu_3SbS_4 film were given as shown in Fig. S3.† It is clear that there exists some excessive

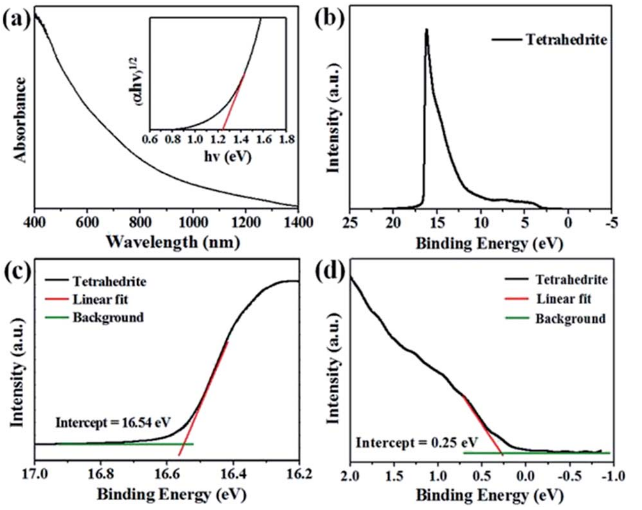

Fig. 7 UV-Vis-NIR absorption spectra and Tauc plots (a) and UPS full spectrum (b) of 2.5 : 1 film. Linear fitting of UPS spectrum in the range of 16.2–17.0 eV (c) and −1.0 to 2.0 eV (d).

driving energy (−0.6 eV) for electron transfer, potentially leading to relatively low theoretical voltage. Thus, it will be desirable to select other N-type electrodes with relatively lower conduction band edge for high open-circuit voltages in the future studies.

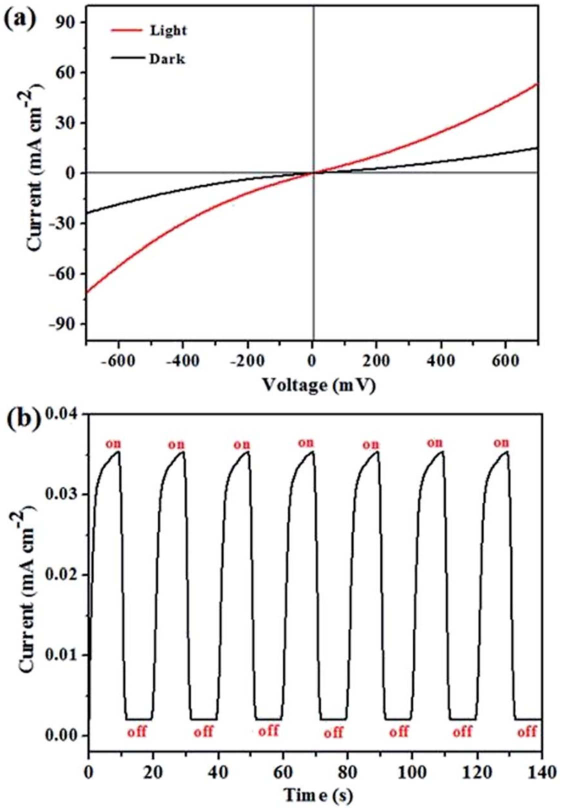

Fig. 8 Current–potential curves (a) and photocurrent response curve (b) under darkness and light for Cu_3SbS_4 device prepared by *in situ* gas–solid reaction method.

Photoresponse performance was investigated to evaluate the quality of the 2.5 : 1 film, and the results are presented in Fig. 8. The current–potential (*I–V*) curves are nearly linear, indicating ohmic contact between silver counter electrode and Cu_3SbS_4 semiconductor. Compared with dark current, the corresponding photocurrent increased remarkably over the entire bias ranged from −700 mV to 700 mV, which is attributed to excited charge carriers by simulated sunlight, leading to high photocurrent. Besides, photocurrent response curve conducted under a bias of 20 mV presents an excellent photoresponse and high photostability. The dark current of 1.96×10^{-3} mA cm^{-2} dramatically rises to 3.50×10^{-2} mA cm^{-2} when the light was on, and the light current drops rapidly as soon as light source was turned off. Despite repeating switch cycle for several times, photocurrent still remains at 3.48×10^{-2} mA cm^{-2} without observable attenuation. Above all, Cu_3SbS_4 made by *in situ* gas–solid reaction method exhibits high photoresponse performance and provides a possibility to be used as photovoltaic absorption layer.

Conclusions

In this report, an *in situ* gas–solid reaction method has been successfully employed for the deposition of pure-phase Cu_3SbS_4 film. Various precursor molar ratios, temperatures, and heating atmospheres have been explored for the deposition. The results show that phase-pure Cu_3SbS_4 can be obtained by the *in situ* gas–solid reaction with the molar ratio of $CuCl_2$ and $SbCl_3$ at 2.5 : 1, and annealing in H_2S at 300 °C. The Cu_3SbS_4 particles with crystal grain sizes of about 3–4 nm are uniformly distributed on the porous TiO_2 film. The Cu_3SbS_4 film shows a broad absorption ranged from 400 nm to 1000 nm with the band gap of 1.24 eV. Moreover, the Cu_3SbS_4 film presents high and stable photoresponse performance, indicating its potential application as solar absorber materials.

Conflicts of interest

There are no conflicts to declare.

Acknowledgements

This work was supported by the 973 Program (No. 2013CB933004), the National Nature Science Foundation of China (Grant No. 61405207, 21174149, 21572235, 51473173, 91433202 and 21221002), and the "Strategic Priority Research Program" of Chinese Academy of Sciences (Grant No. XDA09020000 and XDB12010200). The measurements of (NMR, Mass Spectrometry, XRD, Photoelectron Spectroscopy) were performed at the Center for Physicochemical Analysis and Measurements in ICCAS.

References

1 M. Gloeckler, I. Sankin and Z. Zhao, *IEEE J. Photovolt.*, 2013, **3**, 1389–1393.

2 P. Jackson, D. Hariskos, R. Wuerz, O. Kiowski, A. Bauer, T. M. Friedlmeier and M. Powalla, *Phys. Status Solidi RRL*, 2015, **9**, 28–31.

3 S. C. Riha, B. A. Parkinson and A. L. Prieto, *J. Am. Chem. Soc.*, 2009, **131**, 12054–12055.

4 H. Katagiri, K. Jimbo, S. Yamada, T. Kamimura, W. S. Maw, T. Fukano, T. Ito and T. Motohiro, *Appl. Phys. Express*, 2008, **1**, 041201.

5 A. S. R. Chesman, N. W. Duffy, S. Peacock, L. Waddington, N. A. S. Webster and J. J. Jasieniak, *RSC Adv.*, 2013, **3**, 1017–1020.

6 J. Puthussery, S. Seefeld, N. Berry, M. Gibbs and M. Law, *J. Am. Chem. Soc.*, 2011, **133**, 716–719.

7 M. Wang, D. Xue, H. Qin, L. Zhang, G. Ling, J. Liu, Y. Fang and L. Meng, *Mater. Sci. Eng., B*, 2016, **204**, 38–44.

8 C. Yan, C. Huang, J. Yang, F. Liu, J. Liu, Y. Lai, J. Li and Y. Liu, *Chem. Commun.*, 2012, **48**, 2603–2605.

9 X. Jiang, W. Xu, R. Tan, W. Song and J. Chen, *Mater. Lett.*, 2013, **102**, 39–42.

10 L. Li, X. Liu, J. Huang, M. Cao, S. Chen, Y. Shen and L. Wang, *Mater. Chem. Phys.*, 2012, **133**, 688–691.

11 P. Sinsermsuksakul, K. Hartman, S. B. Kim, J. Heo, L. Sun, H. H. Park, R. Chakraborty, T. Buonassisi and R. G. Gordon, *Appl. Phys. Lett.*, 2013, **102**, 053901.

12 K. T. R. Reddy, N. K. Reddy and R. W. Miles, *Sol. Energy Mater. Sol. Cells*, 2006, **90**, 3041–3046.

13 S. Suehiro, K. Horita, M. Yuasa, T. Tanaka, K. Fujita, Y. Ishiwata, K. Shimanoe and T. Kida, *Inorg. Chem.*, 2015, **54**, 7840–7845.

14 L. Wan, C. Ma, K. Hu, R. Zhou, X. Mao, S. Pan, L. H. Wong and J. Xu, *J. Alloys Compd.*, 2016, **680**, 182–190.

15 T. Rath, A. J. MacLachlan, M. D. Brown and S. A. Haque, *J. Mater. Chem. A*, 2015, **3**, 24155–24162.

16 Y. C. Choi, E. J. Yeom, T. K. Ahn and S. Seok II, *Angew. Chem., Int. Ed.*, 2015, **54**, 4005–4009.

17 L. Wang, B. Yang, Z. Xia, M. Leng, Y. Zhou, D.-J. Xue, J. Zhong, L. Gao, H. Song and J. Tang, *Sol. Energy Mater. Sol. Cells*, 2016, **144**, 33–39.

18 J. Embden, K. Latham, N. W. Duffy and Y. Tachibana, *J. Am. Chem. Soc.*, 2013, **135**, 11562–11571.

19 C. T. Crespo, *J. Phys. Chem. C*, 2016, **120**, 7959–7965.

20 U. Chalapathi, B. Poornaprakash and S.-H. Park, *Ceram. Int.*, 2017, **43**, 5229–5235.

21 K. Aup-Ngoen, T. Thongtem and S. Thongtem, *Mater. Lett.*, 2012, **66**, 182–186.

22 K. Ramasamy, H. Sims, W. H. Butler and A. Gupta, *Chem. Mater.*, 2014, **26**, 2891–2899.

23 L. Yu, R. S. Kokenyesi, D. A. Keszler and A. Zunger, *Adv. Energy Mater.*, 2013, **3**, 43–48.

24 K. Chen, J. Zhou, W. Chen, Q. Chen, P. Zhou and Y. Liu, *Nanoscale*, 2016, **8**, 5146–5152.

25 S. Ikeda, S. Sogawa, Y. Tokai, W. Septina, T. Harada and M. Matsumura, *RSC Adv.*, 2014, **4**, 40969–40972.

26 G. Chen, W. Wang, J. Zhao, W. Yang, S. Chen, Z. Huang, R. Jian and H. Ruan, *J. Alloys Compd.*, 2016, **679**, 218–224.

27 N. D. Franzer, N. R. Paudel, C. Xiao and Y. Yan, in *Photovoltaic Specialist Conference (PVSC), 2014 IEEE 40th*, 2014, pp. 2326–2328.

28 L. Zheng, K. Jiang, J. Huang, Y. Zhang, B. Bao, X. Zhou, H. Wang, B. Guan, L. Yang and Y. Song, *J. Mater. Chem. A*, 2017, **5**, 4791–4796.

29 Y. Zhang, J. Tian, K. Jiang, J. Huang, L. Zhang, H. Wang, B. Bao and Y. Song, *J. Mater. Sci.: Mater. Electron.*, 2017, DOI: 10.1007/s10854-017-7263-1.

30 Y. Zhang, J. Tian, K. Jiang, J. Huang, H. Wang and Y. Song, *Mater. Lett.*, 2017, **209**, 23–26.

31 T. Hurma and S. Kose, *Optik*, 2016, **127**, 6000–6006.

32 C. D. Lokhande, B. R. Sankapal, R. S. Mane, H. M. Pathan, M. Muller, M. Giersig and V. Ganesan, *Appl. Surf. Sci.*, 2002, **193**, 1–10.

33 W. F. Zhang, Y. L. He, M. S. Zhang, Z. Yin and Q. Chen, *J. Phys. D: Appl. Phys.*, 2000, **33**, 912–916.

34 R. Parize, T. Cossuet, O. Chaix-Pluchery, H. Roussel, E. Appert and V. Consonni, *Mater. Des.*, 2017, **121**, 1–10.

35 M. Kundu, T. Hasegawa, K. Terabe, K. Yamamoto and M. Aono, *Sci. Technol. Adv. Mater.*, 2008, **9**, 035011.

36 C. An, Y. Jin, K. Tang and Y. Qian, *J. Mater. Chem.*, 2003, **13**, 301–303.

37 J. v. Embden and Y. Tachibana, *J. Mater. Chem.*, 2012, **22**, 11466–11469.